JOURNAL OF VIROLOGY, June 1996, p. 3797–3806 Vol. 70, No. 6
0022-538X/96/$04.00+0

Crystal Structure of the Top Domain of African Horse Sickness Virus VP7: Comparisons with Bluetongue Virus VP7

AJIT K. BASAK,[1]† PATRICE GOUET,[1] JONATHAN GRIMES,[1]
POLLY ROY,[1,2,3]* AND DAVID STUART[1,4]*

The Laboratory of Molecular Biophysics, University of Oxford, Oxford OX1 3QU,[1] NERC Institute of Virology and Environmental Microbiology, Oxford OX1 3SR,[2] and The Oxford Centre for Molecular Sciences, Oxford OX1 3QT,[4] United Kingdom, and School of Public Health, University of Alabama at Birmingham, Birmingham, Alabama 35294[3]

Received 30 October 1995/Accepted 21 February 1996

The baculovirus-expressed core protein VP7 of African horse sickness virus serotype 4 (AHSV-4) has been purified to homogeneity and crystallized in the presence of 2.8 M urea. The X-ray structure has been solved to a 2.3-Å (1 Å = 0.1 nm) resolution with an R_{factor} of 19.8%. The structure of AHSV VP7 reveals that during crystallization, the two-domain protein is cleaved and only the top domain remains. A similar problem was encountered previously with bluetongue virus (BTV) VP7 (whose structure has been reported), showing that the connections between the top and the bottom domains are rather weak for these two distinct orbiviruses. The top domains of both BTV and AHSV VP7 are trimeric and structurally very similar. The electron density maps show that they both possess an extra electron density feature along their molecular threefold axes, which is most likely due to an unidentified ion. The characteristics of the molecular surface of BTV and AHSV VP7 suggest why AHSV VP7 is much less soluble than BTV VP7 and indicate the possibility of attachment to the cell via attachment of an Arg-Gly-Asp (RGD) motif in the top domain of VP7 to a cellular integrin for both of these orbiviruses.

African horse sickness (AHS) is a gnat (*Culicoides* sp.)-transmitted disease of horses and is endemic in sub-Saharan Africa. Other animals, such as donkeys and goats, are also susceptible. Recently (1988 to 1990) outbreaks of AHS in Morocco, Spain, and Portugal have caused a large number of horse deaths (33, 39). Although nine different serotypes of the AHS virus (AHSV) have been identified in different parts of the world (16, 37), a single serotype, AHSV-4, appears to be responsible for the recent epidemics in Spain and Portugal (28). AHSV belongs to the *Orbivirus* genus of the *Reoviridae* family. The prototype orbivirus of sheep, bluetongue virus (BTV), which is also gnat transmitted, has been studied extensively (51, 52, 54), while limited molecular and genetic information on another gnat-transmitted orbivirus, epizootic hemorrhagic disease virus (EHDV), is also available (18, 52).

AHSV virions contain 10 double-stranded RNA segments coding for seven structural proteins (VP1 to VP7) and three nonstructural proteins (NS1 to NS3). The morphology of purified AHSV particles is essentially identical to that of BTV particles (5, 42). The two viruses have a similar overall structure with a double capsid with a diameter of about 850 Å (1 Å = 0.1 nm) and icosahedral symmetry. Their inner capsid (the core) consists of the viral genome and the major structural proteins VP3 and VP7 along with the minor proteins VP1, VP4, and VP6. The core is surrounded by the outer capsid, consisting of two proteins, VP2 and VP5, which is removed when the virus passes through the cell membrane. Certain cell types can also be infected by cores (41). Electron cryomicroscopy studies at about a 25-Å resolution have shown that the BTV core, which is approximately 700 Å in diameter, is divided into two concentric layers (47): the outer layer, composed of 260 trimers of VP7 forming a T=13 lattice; and the inner layer, composed of a much smaller number of molecules of VP3. In BTV, VP7 trimers form capsomers which are visible in negatively stained images of core particles. Similarly in AHSV, VP7 capsomers can be clearly seen in negatively stained core particles (40a).

AHSV VP7 has 350 residues. Its sequence is highly hydrophobic, having a large number of alanines, methionines, and prolines (53). It can aggregate in infected cells in small flat hexagonal crystals with a maximum dimension of about 6 μm (5, 7). Such crystals have so far never been observed for other orbiviruses. We have recently determined the crystal structure of BTV-10 VP7 at a 2.6-Å resolution (15). The structure is trimeric and fits extremely well in the electron cryomicroscopy maps of the core (15). BTV VP7 has two domains: the bottom domain (residues 1 to 120 and 250 to 349), which has an all α topology and whose base interacts with VP3 in cores; and the top domain (residues 121 to 249), which is an anti-parallel β-sandwich. In order to compare the three-dimensional structures of the VP7 proteins of BTV and AHSV, we have synthesized a recombinant baculovirus harboring the AHSV VP7 gene (7), purified the protein to homogeneity, and grown crystals in the presence of urea to resolve problems of solubility. Unfortunately, the protein was cleaved during the crystallization process, and only the top domain was crystallized. However, this structure gives interesting information about the regions of BTV and AHSV VP7 which might interact with the cell membrane when cells are infected by cores. It also highlights patches on the molecular surface with differences in hydrophilicity between BTV and AHSV VP7.

* Corresponding author. Mailing address for Polly Roy: NERC Institute of Virology and Environmental Microbiology, Mansfield Rd., Oxford OX1 3SR, United Kingdom. Mailing address for David Stuart: Laboratory of Molecular Biophysics, University of Oxford, Rex Richards Bldg., South Parks Rd., Oxford OX1 3QU, United Kingdom.

† Present address: Department of Crystallography, Birbeck College, London, WC1E 7HX, United Kingdom.

MATERIALS AND METHODS

Synthesis and purification of the protein. The full-length cDNA of the AHSV-4 double-stranded RNA segment 7 (S7) encoding the VP7 protein has been

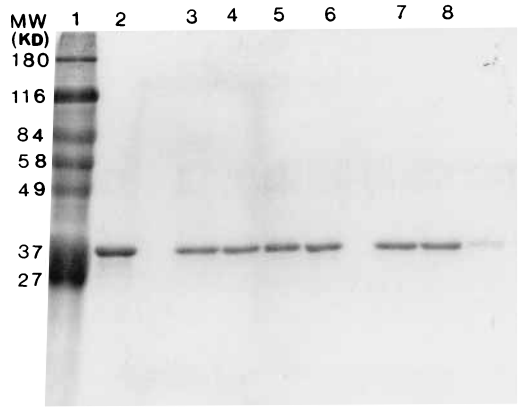

FIG. 1. Analysis of recombinant AHSV-4 VP7 protein by SDS-PAGE (10% polyacrylamide). Lanes: 1, marker; 2, protein after the first step of purification in a sucrose gradient; 3 to 8, fractions of pure protein after the second step of sucrose gradient. MW, molecular mass.

cloned, sequenced, and expressed in a baculovirus vector (7). Insect cells (*Spodoptera frugiperda*) were infected with the recombinant baculovirus AcAHSV-4.7, which synthesizes the AHSV-4 VP7 protein. The infected cells were harvested after an incubation period of 72 h at 28°C, pelleted by centrifugation at $320 \times g$ at 4°C, and rinsed in phosphate-buffered saline. The cells were then lysed at 6×10^7 cells per ml in lysis buffer (10 mM Tris-HCl [pH 7.8] buffer, 150 mM NaCl containing 5 mM EDTA and 0.5% Nonidet P-40) and incubated on ice for 15 min. Cell nuclei were removed from the cell lysate by centrifugation at $160 \times g$ for 10 min. In order to recover the maximum amount of crude protein, the process of cell lysis and extraction of cytoplasmic fraction was repeated three or four times. The extract was then loaded onto a 20 to 80% (wt/vol) continuous sucrose gradient in 0.2 M Tris-HCl (pH 7.5). The gradients were centrifuged at $116{,}000 \times g$ for 3 h at 4°C in an SW41 (Beckman) rotor, and 1-ml fractions were collected. The fractions containing the protein were pooled and diluted (1:2) with 0.2 M Tris-HCl (pH 7.5) and recentrifuged on a 40 to 80% (wt/vol) step gradient in the same buffer at $116{,}000 \times g$ for another 3 h at 4°C. The fractions containing the AHSV-4 VP7 were pooled and dialyzed overnight at 4°C in 10 mM Tris-HCl (pH 7.5). The purity of the protein was finally checked using by sodium dodecyl sulfate–10% polyacrylamide gel electrophoresis (SDS-PAGE) (Fig. 1).

Crystallization. The solubility of AHSV VP7 in the dialyzed fractions was limited to 0.2 to 0.4 mg/ml. A number of detergents were added to the protein in an effort to improve its solubility, but without success. Finally, the solubility was improved by dialyzing the protein fractions at 4°C against 10 mM Tris-HCl (pH 7.5), containing increasing amounts of urea. The urea concentration was increased stepwise, in steps of 0.5 M, to a final concentration of 2.8 M. The protein could then be concentrated with a Centricon concentrator (with a 10-kDa exclusion membrane) to a final concentration of 6 to 8 mg/ml.

Crystallization conditions were first screened by the broad screening method of Jancarik and Kim (19). The conditions were then refined, and good-quality crystals were grown at 20°C by the sitting drop vapor diffusion method (38). The precipitant solution in the reservoir was a 45 to 48% saturated ammonium sulfate in 10 mM Tris-HCl (pH 7.8). The protein was mixed with the well buffer in a ratio of 1:1 and left to equilibrate with the reservoir solution. Crystals appeared within a period of 2 to 3 weeks. The number of nucleation sites was controlled by using 2 to 4% dioxane as an additive. The largest crystals achieved a size of 0.8 by 0.5 by 0.5 mm^3 over a period of 8 to 12 weeks (Fig. 2).

X-ray analysis. The crystals were tested first with an in-house 18-cm-diameter Marresearch imaging plate mounted on a Rigaku RU200H rotating anode X-ray generator operating at 60 kV (70 mA). The crystals diffracted beyond 2.6 Å, and a native data set to a resolution of 3.0 Å was collected as a series of images, each spanning a 0.5° rotation. Data were analyzed with the programs XDS (22, 23) and MOSFLM (31), indicating that the space group was I4 with unit cell parameters of $a = b = 157.2$ Å, $c = 57.7$ Å, $\alpha = \beta = \gamma = 90°$. Data processing statistics are presented in Table 1.

A self-rotation function calculated with the program X-PLOR (4) showed a strong feature on the $\kappa = 180°$ section, consistent with the presence of two molecules in the asymmetric unit related by a noncrystallographic twofold axis. This would correspond to a solvent content of 53% in the crystal with two monomers in the asymmetric unit (36). This was surprising, since the VP7 molecule is trimeric (15); however, it seemed possible that the presence of urea in the solution had caused dissociation of the molecule during crystallization. Subsequently, a native data set to a resolution of 2.3Å was collected at the Photon Factory, KEK, Tsukuba, Japan, on station BL-6A2 by using the Sakabe Weissenberg camera (56, 57). The crystal-to-detector distance, coupling constant, exposure time, and oscillation step were 430 mm, 0.8° mm^{-1}, 160 s, and 4°, respectively. Diffraction patterns were recorded on a detection surface formed by pairs of 200-by-400-mm^2 Fuji BAS-III imaging plates and data readout was carried out off-line with a Fuji BA100 IP scanner. The data were processed with the program package DENZO (45) (Table 1). A final set of reflections was obtained by merging the unique set of in-house data with the Photon Factory data by using the programs ROTAVATA and AGROVATA of the CCP4 suite (5a) (Table 1).

Phasing and molecular replacement. We first attempted to solve the structure by molecular replacement by using the in-house X-ray diffraction data and the BTV VP7 structure previously determined (15). The two sequences show an identity of 43% (Fig. 3), and hence we would expect the root-mean-squared (rms) deviation in C positions to be less than 1 Å (6). The program AMoRe (43) was used, but no convincing solution could be found with either the complete BTV VP7 monomer or either of the two domains of the monomer. It was supposed that this might be due to some structural changes caused by the presence of 2.8 M urea, and it was decided to solve the structure by using heavy atom methods. AHSV VP7 crystals were soaked in a variety of gold, lead, mercury, platinum, or uranium compounds. Data were collected in-house to a 3.5-Å resolution. The positions of the heavy atoms were found with GROPAT (21) and refined with MLPHARE (44). The best results were obtained with an ethyl mercury chloride derivative, and it was decided to attempt a single isomorphous replacement analysis (Table 1). Six heavy atom positions per asymmetric unit were detected, and solvent flattening was performed with the GAP program (15a) and the CCP4 programs (7a). This process converged to give a reciprocal space correlation coefficient of 0.95 and an R_{factor} of 17% between observed data and data obtained by inversion of the solvent-flattened map. Inspection of this map on a graphics workstation revealed a threefold axis relating domains rich in β-strands. It was immediately apparent that only the top domain of the protein had been crystallized and that crystals contained one top trimer fragment per asymmetric unit. On this basis, the solvent content of the crystals was calculated to be about 64%.

Molecular replacement was performed again with AMoRe, by using the BTV VP7 trimer top domain as a model and deleting side chain atoms beyond C_β. A solution was obtained with an R_{factor} of 44% to a 4-Å resolution. This solution agreed well with the map obtained by single isomorphous replacement, and it was found subsequently that the heavy atom sites corresponded to two mercury atoms per subunit bound to the sulfur atoms of residues Cys-161 and Cys-195, respectively.

Structure refinement. Refinement was performed with the program X-PLOR (4), initially with noncrystallographic constraints, and reflections with Bragg spacings of between 15 and 3 Å and with $F > 2$ (σF). Side chains were positioned in the $2F_{obs}$-F_{calc} electron density maps with the graphics program TURBO-FRODO (50). After several cycles of simulated annealing and positional refinement, a model with an R_{factor} of 22% between 15 and 3 Å was obtained. The electron density suggested that the fragment started at Gly-127 and ended at Tyr-250. At this stage, the merged set of in-house and Photon Factory data was used to extend the refinement to a 2.3-Å resolution. Positional refinement was carried out with the new set of data, but it converged with a rather high R_{factor} of 27% for data with $F > 2(\sigma F)$ in the range 15 to 2.3 Å. At this stage, it became clear from the electron density that the noncrystallographic threefold axis was not strictly obeyed and noncrystallographic symmetry (NCS) restraints were applied instead of strict constraints, allowing a decrease in the R_{factor}, but only to 25%. The refinement was therefore performed with the three subunits refined independently, producing a drop in the R_{factor} to 22%. In the absence of noncrystallographic restraints, there were three observations per degree of freedom, so the refinement was still well conditioned. Water molecules were added grad-

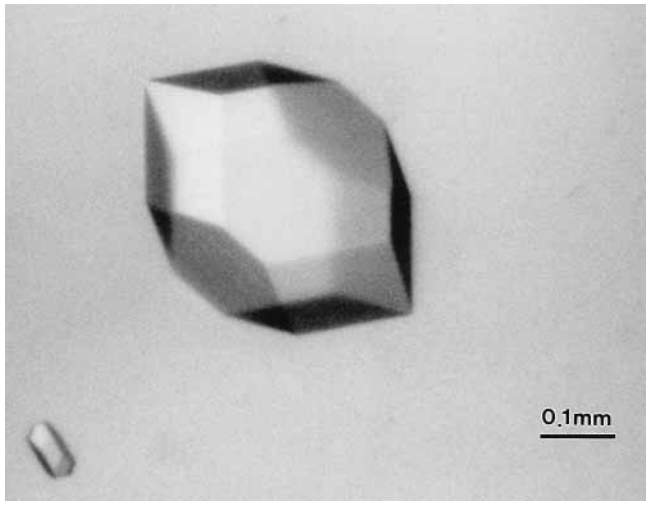

FIG. 2. Crystals of the AHSV VP7 fragment.

ually, and a final model was obtained with 61 water molecules per monomer, an R_{factor} of 19.8% for data with $F > 2$ (σF) between 15 and 2.3 Å (the R_{factor} is 21% for all data), and good geometry (Table 2). An error in the sequence was revealed during the refinement of the structure. It was not possible to position the segment Ala-208–Pro-209–Gly-210, which was supposed to be an insertion in AHSV compared with the sequence of BTV, in the electron density maps. In fact, this segment was simply an erroneous duplication of the preceding Ala-Pro-Gly tripeptide. The corrected AHSV VP7 sequence is presented in Fig. 3.

Other programs used in the study of the structure of the fragment. The determination of the secondary structure of the AHSV VP7 fragment was carried out with the program DSSP (24). Superposition analyses were performed with TURBO-FRODO. Studies of the molecular surface and cavities were done with the program VOIDOO, with a probe-accessible radius of 1.4 Å (25); and the program MS, available in the TURBO-FRODO package (8). An analysis of the difference in hydrophilicities between BTV and AHSV VP7 surfaces was made as follows. (i) The hydrophilicities of corresponding residues in BTV and AHSV VP7 were calculated with the algorithm of Kyte and Doolittle (27), which is based on the amino acid sequence. (ii) The difference in hydrophilicity between BTV and AHSV VP7 was calculated with respect to each BTV VP7 residue. (iii) The accessible surface of BTV VP7 was computed with a probe radius of 2.5 Å by the MS program and displayed on the graphics station. (iv) The resulting surface was colored according to the difference in hydrophilicity between BTV and AHSV VP7.

Nucleotide sequence accession numbers. The coordinates of the AHSV VP7 fragment and the observed structure factors have been deposited in the protein data bank under the codes 1ahs and r1ahssf, respectively.

RESULTS AND DISCUSSION

AHSV VP7 general structure and superposition with BTV VP7. The building block for the AHSV VP7 crystals is a trimeric fragment of the trimeric molecule (Fig. 4) containing three subunits named A, B, and C. Each subunit shares the jelly roll topology of the BTV VP7 top domain (15) (Fig. 5) and contains the homologous residues. The whole trimeric AHSV VP7 fragment can be packed into a parallelepiped with the dimensions 55 by 55 by 40 Å, the last dimension being along the molecular pseudo-threefold axis. $2F_{obs}$-F_{calc} maps contoured at 1σ above the mean electron density indicate that monomer A starts at Gly-127 and ends at Thr-251. The segment from Arg-177 to Ala-181 (segment 177–181) does not appear in the electron density maps and has not been modelled. Subunit B starts at Thr-126 and ends at Tyr-250. This fragment is continuous, but only the backbone of segment 177–180 has been modelled. Subunit C starts at Gly-127 and ends at Tyr-250. The segment Pro-176 to Ala-181 has not been modelled. The problematic segment, 176–181, is located at the protein surface in the same region as the N and C termini (Fig. 4). Since there is considerable disorder in this region, the electron density maps cannot be relied upon to give the exact number of residues in the fragment. There is nothing unusual either in the electron density maps or in the protein geometry which can be attributed to the presence of urea in the crystallization solution.

The A, B, and C subunits can be superimposed upon each other with an rms deviation of 0.3 Å between C_α atoms. This value is similar to the estimation of the mean error on atomic positions obtained from a Luzatti plot (34), and the relative rotation relating adjacent subunits is almost exactly 120°. However, the drop in the R_{factor} when the three subunits are refined independently shows that the three subunits are not related by a true molecular threefold axis. The deviation from exact symmetry is particularly clear in differences in electron density between segment 176–181 in subunit B and those in subunits A and C. The analysis of the crystal packing given in the next section explains why the 176–181 segment is less disordered in subunit B than in subunits A and C.

The AHSV and BTV VP7 top domains can be superimposed with an rms deviation of 1.2 Å between all equivalent C_α atoms (Fig. 6). The C_α traces of the two domains differ mainly at their molecular surface near zones of inclusion or deletion in the sequence (Table 3). Strand βA of subunit A, which is parallel to strand βD of subunit C in BTV VP7, is not found in AHSV VP7, and the helix η_1, which is a short 3_{10} helix in BTV VP7, is more like the α helix in AHSV VP7. These structural differences are, however, very minor, and we have no doubt that the bottom domains of AHSV and BTV VP7 are also extremely similar.

Molecular contacts in AHSV VP7 crystals. There is a considerable amount of solvent in the AHSV VP7 crystals (64%), and large channels with diameters of 70 and 20 Å are found along the crystallographic **c** axis. This is likely to explain the relatively high mean B_{factor} of the fragment (37 Å^2). One AHSV VP7 fragment is in contact with four other fragments, and two types of crystallographic interfaces can be described (Table 4; Fig. 7): interface I, which relates subunits B via con-

TABLE 1. Processing statistics

Data set	Data collection site	Resolution (Å)	Collected reflections (no.)	Completeness (%)	$I > 3\sigma(I)$ (%)	Unique reflections (no.)	R_{sym} (%)[a]	R_{merge} (%)[a]	Phasing power on centrics (acentrics)[b]	R_{cullis} on centrics (acentrics)[c]
Native										
1	In house, 1993	30–3.0	51,063	95	82	13,535	10.0			
2	Photon Factory, 1993	30–2.3	63,616	87	69	27,140	5.1			
Merged		30–2.3		93	71	29,456		8.9		
EMC derivative	In house, 1994	30–3.5	22,679	92	81	8,220	9.5		1.1 (1.5)	0.6 (0.2)

[a] R_{sym} and R_{merge} were determined by the equation

$$R = \sum_{hkl} \sum_{j} | I_{hkl,j} - \langle I_{hkl} \rangle | / \sum_{hkl} \sum_{j} I_{hkl,j}$$

where h, k, and l are the indices for unique reflections and j is the index for symmetry redundant reflections. R_{sym} is accordingly the R_{value} for symmetrically related reflections of a single data set, and R_{merge} is the R_{value} for the merged data set. I are the collected intensities. Intensities (I) and structure factors (F) are related by the equation $I = F^2$.

[b] Phasing power is the rms value of the heavy atom structure factor amplitude (FH) divided by the rms lack of closure error.

[c] R_{cullis} was calculated by the equation

$$R_{cullis} = \sum_{hkl} \Big| |\mathrm{FPH}_{obs}|_{hkl} - k|\mathrm{FPH}_{calc}|_{hkl} \Big| / \sum_{hkl} |\mathrm{FPH}_{obs}|_{hkl}$$

where FPH is the derivative structure factor amplitude and k is a scale factor.

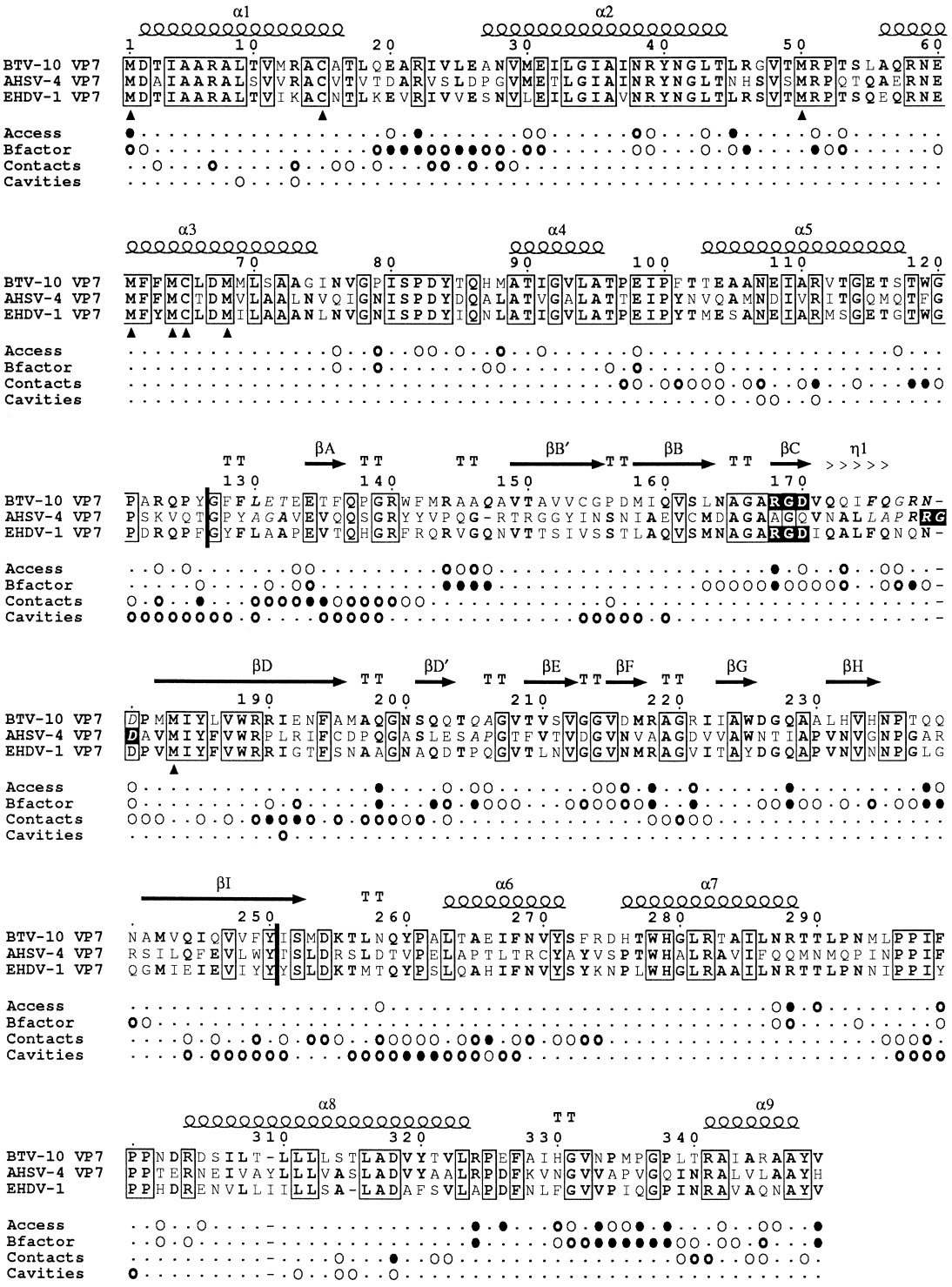

FIG. 3. Alignment of three sequences of protein VP7 of orbiviruses taken from the SWISSPROT bank (3). AHSV had 43% identity with BTV VP7; the sequence of the crystallized fragment is delimited with bold vertical lines at positions Gly-127 and Tyr-250. EHDV had 64% identity with BTV VP7. Residues conserved in all three of the sequences are boxed, those conserved in at least two sequences are in boldface, and the RGD tripeptide is boxed in black (see text section 5). C_α atoms of AHSV VP7 and BTV VP7 separated by a large distance after superposition with TURBO-FRODO are in italic (Table 3 and Fig. 5). The first line shows the secondary structure of BTV VP7 as calculated with DSSP (24). α Helices are indicated by spirals, β strands are indicated by arrows, 3_{10} helices are indicated by output signs, and β turns are indicated by boldface **T**. Conserved cysteines are indicated by solid triangles drawn below the EHDV sequence. Some structural properties of BTV VP7 are given below the sequence alignment. Access, solvent accessibility per residue for the whole trimer calculated with DSSP. Accessibility in the range 70 to 100 Å^2 is indicated by ○, that in the range 100 to 130 Å^2 is indicated by ○, and that above 130 Å^2 is indicated by ●. Bfactor, residues with an average B_{factor} in the range 30 to 40 Å^2 are indicated by ○, those in the range 40 to 50 Å^2 are indicated by ○, and those above 50 Å^2 are indicated by ●. Contacts, minimum atomic distance between two residues of adjacent subunits. Minimum distances in the range 4 to 3.4 Å are indicated by ○, those in the range 3.4 to 2.8 Å are indicated by ○, and those below 2.8 Å are indicated by ●. Cavities, residues lining the biggest cavities in the trimer after calculation with VOIDOO (Fig. 8). Residues lining only the second biggest cavity are indicated by ○, those lining only the biggest cavity are indicated by ○, and those lining both of these cavities are indicated by ●.

TABLE 2. Structure statistics

Parameter	Value
Resolution range (Å)	15–2.3
No. of reflections with $F>2\sigma(F)$	25,822
Completeness (%)	82
No. of non-hydrogen atoms per trimer	2,728
R_{factor} [a]	19.8
Mean B_{factor} on main chain (Å^2)	34
rms deviation from ideality on bond lengths (Å)[b]	0.018
rms deviation from ideality on bond angles (°)[b]	2.2

[a] R_{factor} was determined by the equation

$$R_{factor} = \sum_{hkl} \left| |F_{obs}|_{hkl-k} - |F_{calc}|_{hkl} \right| / \sum_{hkl} |F_{obs}|_{hkl}$$

where k is a scale factor.

[b] Parameters for energy minimization are taken from file "parhcsdx.pro," courtesy of R. Engh and R. Huber, and are included in the X-PLOR package.

tacts between the 178–182 and 226–228 loops and the CHEF sheet, and interface II which relates subunits A and C via contacts between their CHEF sheets. On this basis, we conclude that crystallographic contacts stabilize the flexible segment 176–182 of subunit B, while in subunits A and C, this loop is completely exposed to the solvent (Fig. 7, bottom), explaining the observed differences in the electron density maps described above.

The crystallographic interfaces I and II are mostly made by hydrophobic contacts. It has been reported for the crystallization of the core of human immunodeficiency virus type 1 integrase that the replacement of a single hydrophobic residue by a hydrophilic one can dramatically increase the solubility of the protein and render the material suitable for crystallization (9). A similar approach for the highly hydrophobic AHSV VP7 might allow urea to be eliminated from the crystallization medium. Making the reasonable assumption that the hydrophobic residues involved in the crystallographic contacts contribute to the tendency of the protein to aggregate, we suggest two AHSV VP7 residues that could be mutated to increase solubility: Ala-167 and Phe-209 (which replace BTV VP7 Arg-168 and Thr-209, respectively). These residues are found in both interfaces I and II and increase the hydrophobicity of AHSV VP7 compared with that of BTV VP7.

Properties of the molecular surface and cavities. In order to understand the difference in solubilities between AHSV and BTV VP7, we have analyzed the difference in hydrophobicities between the molecular surfaces of the two trimers, using the complete sequence of BTV and AHSV VP7 to calculate a difference of hydrophobicity between the two proteins (see Materials and Methods). Figure 8 shows the result, essentially a difence hydrophobicity plot, mapped to the solvent-accessible surface of the molecule. Since the orientation of the VP7 trimer in the mature core has been determined by correlation of the X-ray and electron cryomicroscopy analyses (15), we can analyze the changes in terms of the functions of the various surfaces. According to Fig. 8, the base of BTV VP7, which is in contact with VP3 in the virus, is more hydrophobic, while its upper part, which is in contact with the VP2/VP5 outer capsid in the virus, seems slightly more hydrophilic. We assume that these changes reflect complementary changes on the other proteins involved in these interactions. More interestingly, a large hydrophilic area comprising both strand C and helix η_1 of subunit A and C-terminal helix 9 of subunit B is seen running down the edge of BTV VP7. Since most of this region is not involved in protein-protein interactions in the core particle, it is not clear what the biological significance of these changes is. One possible role is in interaction with a cellular receptor for the core. This is discussed below. Arg-168, whose equivalent, AHSV VP7 Ala-167, is a candidate for a solubility mutation, is part of this hydrophilic area. An Ala-167–Arg change is therefore a strong candidate for increasing the solubility of AHSV VP7.

BTV VP7 contains two major cavities lying along the molecular threefold axis: the first, with a volume of 1,950 Å^3, extends from the upper part of the bottom domain to one-half of the top domain; and the second, with a volume of 750 Å^3, is surrounded by helices of the bottom domain (Fig. 9). The cleavage of the top domain in the AHS VP7 fragment occurs at about halfway down the biggest cavity, at a point at which the cavity surface approaches to within 5 Å of the outer surface of the molecular envelope. Further discussion of the cleavage site is presented in the next section.

An unidentified atom. Among the 61 water molecules positioned in the fragment, one located along the threefold molecular axis and also found in BTV VP7 is worthy of note. This molecule, named Wat1 (Fig. 4 and 10), has six electrostatic contacts with the nitrogen atoms of surrounding arginines and glutamines. These characteristics suggest an anion, whereas the observed octahedral geometry is similar to the coordination of Mg^{2+} by proteins (30). Furthermore, Wat1 refines to a B_{factor} of 2 Å^2, while surrounding residues have an average B_{factor} of about 20 Å^2, suggesting that there are actually considerably more electrons present than are found in a single water molecule. The program ASSAM was used to see if the unusual constellation of residues observed around Wat1 has been observed in other proteins (1a). Several proteins in which a phosphate or a sulfate is bound to a group of three arginines were detected. However, both phosphate and sulfate ions are

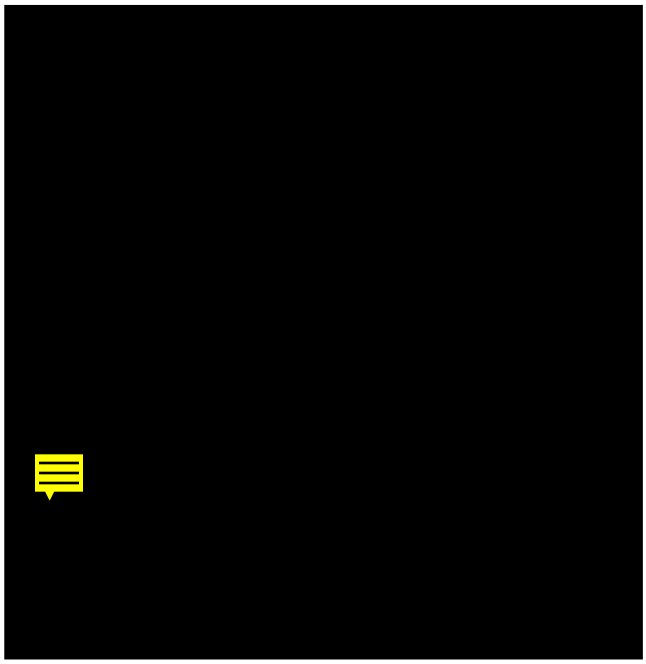

FIG. 4. VP7 chimera represented with the coordinates of BTV VP7 for the bottom domain and of the crystallized fragment of AHSV VP7 for the top domain. Monomer B of the fragment is drawn in a ribbon mode, highlighting its secondary structure. Coils are in orange, strands are in green, and helices are in cyan. The rest of the chimera is represented by a C_α trace, with a different color for each monomer (red, green, and blue). The colors of the top domain are paler than the colors of the bottom domain. Wat1, which is discussed in the text, is a molecule located along the molecular threefold axis. The figure was drawn with MOLSCRIPT (26) as modified by R. Esnouf and rendered with RASTER3D (40).

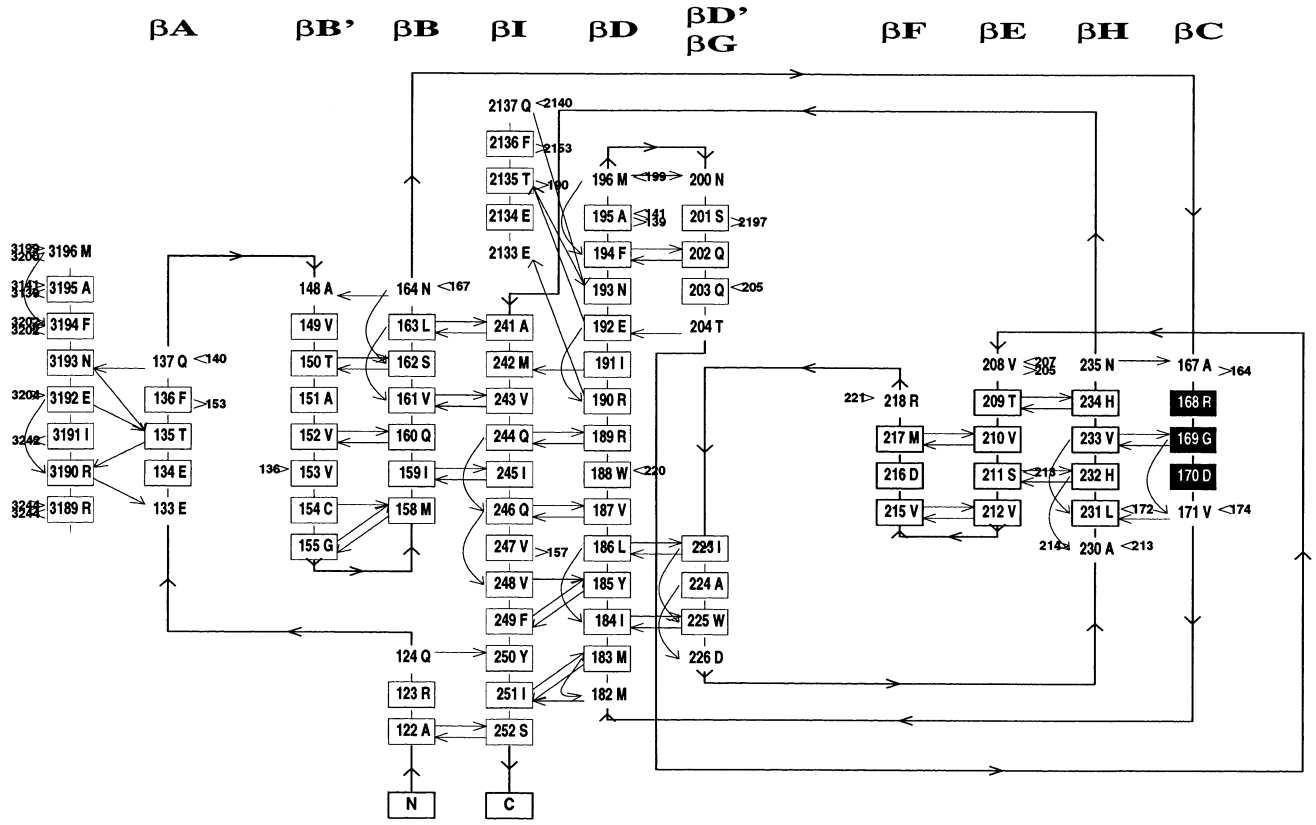

FIG. 5. Hydrogen bonding diagram of the jelly roll of BTV VP7. NH-CO bonds are indicated with arrows. The RGD tripeptide, which may be crucial for an attachment of the protein with a cell receptor, is boxed in black (see text section 5). Figure was drawn with HERA (17).

too big to fit in the Wat1 site. A fluoride (F^-) would be electronically sensible and refines to a B_{factor} of 8 Å^2. However, it is unlikely that in the virus each VP7 protein contains a fluoride ion. A chloride (Cl^-) does increase the B_{factor} of Wat1 but also, unfortunately, slightly increases the R_{factor} of the model. Perhaps the most likely explanation is that Wat1 is usually a hydroxyl but is partially replaced by a chloride ion in the crystal. Indeed, in the EMC derivative, the extra density in Wat1 disappears, while three extra densities appear nearby, which correspond to mercury atoms bound to the cysteine 195 of each subunit, demonstrating that diffusion of molecules in and out of this site is possible. While the biological significance of this ion, if any, remains unclear, ions (albeit usually cations) have been observed frequently on symmetry axes in virions and have been implicated in the assembly-disassembly processes (48). The nature and role of this ion therefore warrant further investigation.

The cleavage site. In addition to the structure of the intact BTV VP7 previously reported (15), we have also determined the structure of a trimeric fragment of the top domain of BTV VP7 protein (14). This cleavage at the junction between the two domains bedeviled our initial analysis of the VP7 structure (3a, 14), but we were able to solve the problem by adding a cocktail of protease inhibitors to the crystallization solution. AHSV VP7 crystals were also grown in presence of inhibitors; however, this did not solve the problem. The BTV fragment appears to start at Gly-127 and end at Tyr-250; i.e., it is essentially the same fragment as that observed for AHSV. Although we cannot be sure of the exact sites of cleavage, it is interesting

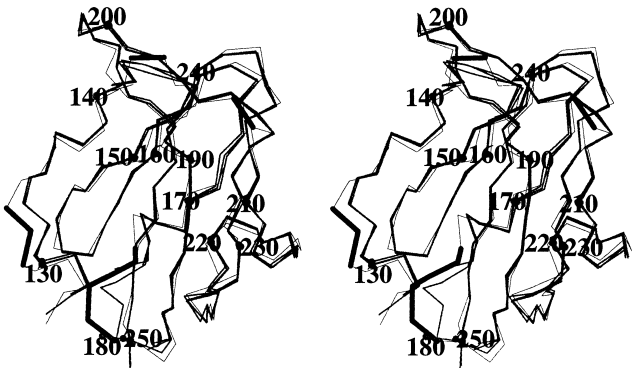

FIG. 6. Superimposition of the C_α traces of the monomer B of the AHSV VP7 fragment (medium lines) and of a monomer of the BTV VP7 top domain (thin lines). Zones of maximum deviation between the two traces are highlighted by thick lines (Table 3). The stereo view was drawn with MOLSCRIPT.

TABLE 3. Zones of maximum deviation between AHSV VP7 and BTV VP7

Characteristic	VP7 zone of maximum deviation (Å)	
	AHSV	BTV
β-Turn	131–133	131–133
Deletion in AHSV VP7		146
Insertion in AHSV VP7	174–180	175–180
β-Turn	205–206	205–206

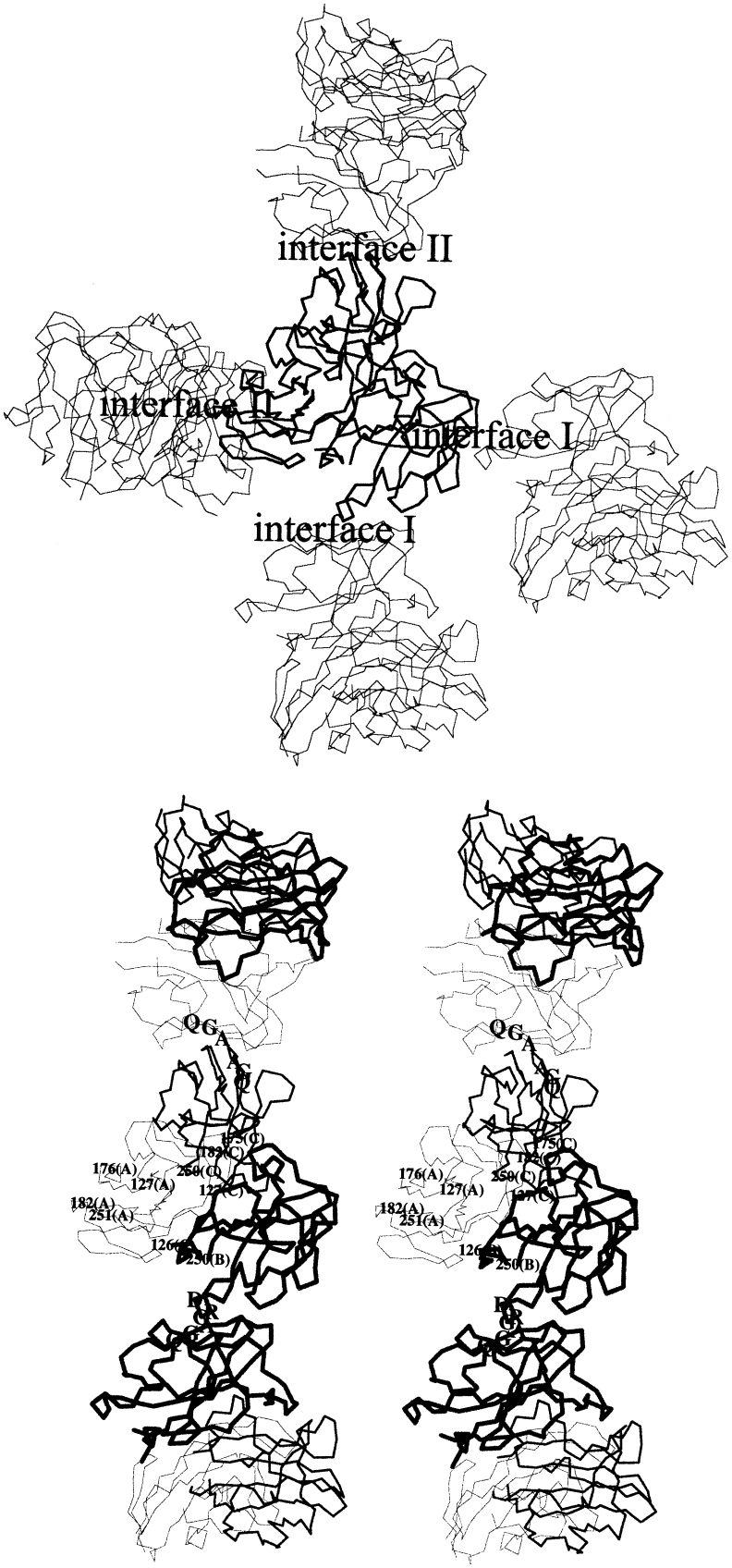

FIG. 7. Position of the crystallographic interfaces around one fragment. (See Table 4 for a list of the interatomic distances between monomers related through the crystallographic symmetry.) (Top) Interfaces, with one fragment highlighted by a C_α trace (bold lines). (Bottom) Interfaces, with monomers A, B, and C highlighted by thin, thick, and medium lines, respectively. The positions of the 175–182 flexible loop and of the tripeptides Ala-167–Gly-168–Gln-169 and Arg-178–Gly-179–Asp-180 are indicated (see text section 5).

TABLE 4. Crystal contacts between fragments to a distance of 4 Å

Interface	Subunit	Residue	Subunit	Residue	No. of contacts
1	B	Arg-178	B	Asn-216	3
	B	Gly-179	B	Phe-209	7
	B	Gly-179	B	Thr-211	1
	B	Ala-181	B	Phe-209	1
	B	Val-182	B	Gly-165	1
	B	Val-182	B	Ala-166	1
	B	Val-182	B	Pro-236	5
	B	Asn-226	B	Pro-236	2
	B	Ile-228	B	Pro-236	1
	B	Ile-228	B	Gly-207	1
	B	Ile-228	B	Pro-236	1
2	A	Arg-147	C	Asp-163	8
	A	Arg-147	C	Ala-164	3
	A	Arg-147	C	Gly-165	1
	A	Gly-165	C	Ala-166	1
	A	Gly-165	C	Ala-167	5
	A	Ala-166	C	Gly-165	3
	A	Ala-166	C	Ala-167	3
	A	Ala-167	C	Gly-165	5
	A	Ala-167	C	Ala-166	1
	A	Ala-167	C	Ala-167	1
	A	Ala-167	C	Pro-236	1
	A	Gly-168	C	Pro-236	3
	A	Gln-169	C	Pro-236	1
	A	Phe-209	C	Asn-232	2
	A	Gly-214	C	Asn-216	6
	A	Asn-216	C	Gly-214	3
	A	Asn-232	C	Phe-209	3

that Gly-127 and Tyr-250 are strictly conserved among orbiviruses (Fig. 3). A mechanism of autoproteolysis has been proposed as a maturation mechanism for other viral proteins (49, 58), and it is possible that a similar process occurs in VP7, triggered in this case by the crystal growth. An automatic search performed among orbivirus sequences against those in the PROSITE database (45) detected no motif for the protease site in the cleavage region of VP7. Gly-127 and Tyr-250 are separated by more than 5 Å, which is rather distant for a concerted mechanism. Inspection of the environment of the cleavage sites in the context of the intact BTV VP7 gives no real clue as to the mechanism at work, and the sites are not readily accessible to proteases. The implication is that the provision of flexibility in this region is a functional imperative. Further work is required to identify a particular biological role for this flexibility or for the cleavage of VP7.

FIG. 8. Difference in hydrophilicities at the solvent-accessible surface between BTV and AHSV VP7. A color scale is given on the figure, going from blue (BTV VP7 strongly more hydrophilic) to red (BTV VP7 strongly more hydrophobic). In the virus, the top of VP7 is in contact with the VP2/VP5 layer while the bottom is in contact with the VP3 layer. Figure was drawn with TURBO-FRODO (for more details, see Materials and Methods).

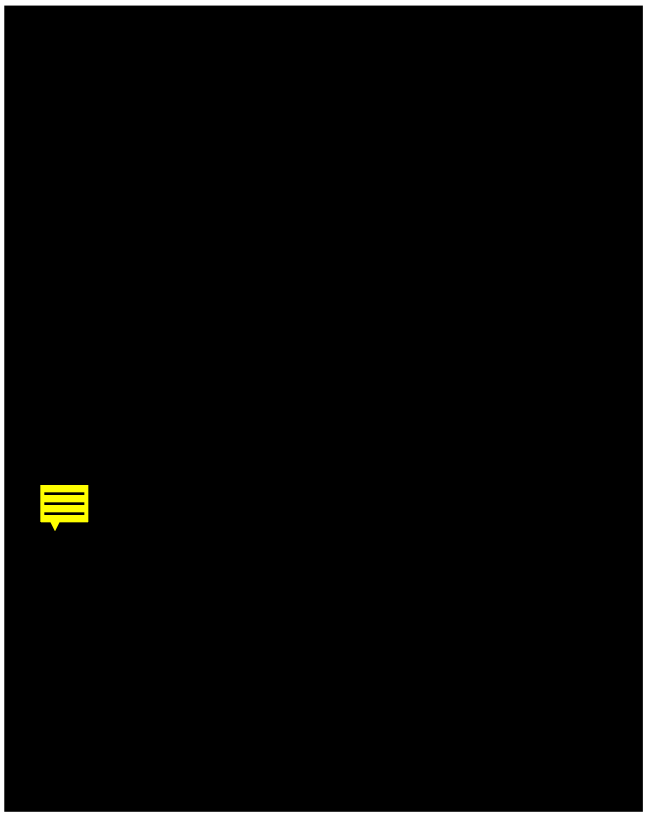

FIG. 9. Slice of the solvent accessibility map of BTV VP7 showing the internal cavities and the narrowing at the cleavage zone. The C_α trace of one monomer is drawn in grey, with the extremities of the top domain fragment, Gly-127 and Tyr-250, in red. Lys-255 is a residue which seems important for assembly of the virus (61). The solvent map was calculated with MS with a probe radius of 2.5 Å and rendered with TURBO-FRODO.

The RGD motif. Ala-167, Gly-168, and Gln-169 replace the BTV VP7 segment Arg-168–Gly-169–Asp-170 (RGD), which has been suggested as a possible determinant for attachment of BTV VP7 to a cell surface receptor (15). Indeed, it is known that BTV cores are able to pass through the cell membrane and can compete against foot and mouth disease virus for its cellular receptor, an integrin (7b). The RGD motif is involved in the attachment of foot and mouth disease virus to integrins (11, 32, 35) as well as for the attachment of other biological systems to cells (46, 55). The crystal structure of an integrin I domain has recently been determined at a 1.7-Å resolution (30). This structure revealed an accessible divalent cation site, as had been proposed earlier (1), which is thought to play a key role in protein binding. Indeed, completion of the coordination sphere of an integrin-bound Mg^{2+} by a carboxylate oxygen of the aspartic acid of the RGD motif is likely to be a key event

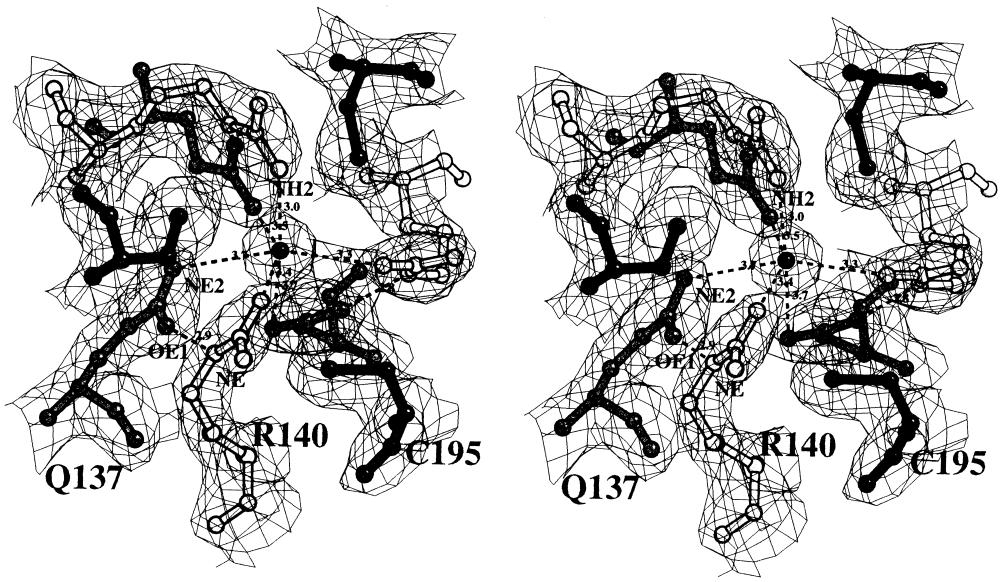

FIG. 10. Residues surrounding the singular molecule Wat1. The $2F_{obs}$-F_{calc} electron density map is also represented at a 1σ level at 2.3-Å resolution. The stereo view was drawn with MOLSCRIPT and TURBO-FRODO.

in the integrin-ligand recognition. Since in cases in which a motif other than RGD is used for integrin recognition an acid residue has always been implicated (20), we feel that the AGQ sequence of AHSV is unlikely to play the same role as that proposed for the RGD sequence in BTV. However, we note that AHSV VP7 does have an RGD motif, in a slightly different position (residues 178 to 180) on the highly flexible loop, segment 175–180 (Fig. 4, 6, and 7, bottom). This loop is located at the lower part of the top domain and is likely to be somewhat less accessible to integrins than the AGQ 167–169 segment. To see if the interaction of an AHSV core with the integrin domain is feasible in the context of the whole core, we have performed a modelling exercise. The BTV and AHSV VP7 structures and the structure of the AHSV VP7 chimera have been fitted to the cryomicroscopy electron density maps of BTV cores, and the structure of the integrin domain has been docked onto this model for the virus core with a graphics workstation. Since the I domain represents only a small fraction of the complete integrin, these results must be interpreted with caution. In the case of BTV, the RGD is positioned such that docking is straightforward, with the I domain facing into large channels on the core surface, so that a much larger molecule could be accommodated. Since the RGD of AHSV VP7 lies somewhat deeper into the core, the modelling is more constrained; however, the rearrangement of this region observed in the structure in AHSV allows plausible docking. There is a consensus that integrin-binding RGD motifs often occur on flexible loops (32), and the RGD loop is certainly one of the most flexible parts of the AHSV VP7 domains.

Conclusion. This study shows that the VP7 molecules of orbiviruses remain trimeric in relatively high concentrations of urea, and the structure of the protein is not significantly perturbed. This may be a generally useful way of studying the structures of relatively insoluble viral coat proteins. The structures of VP7 molecules are, as expected, highly conserved across related orbiviruses. We suggest that Ala-167 may contribute significantly to the insolubility of AHSV VP7 and that mutation of this residue may improve the solubility of the protein. This residue is also of particular biological interest, since Ala-167 replaces BTV Arg-168, which is a part of the RGD motif in BTV. RGD domains in biological systems are very often involved in the binding of molecules to the cell membrane. The assembly of recombinant VP3 and VP7 molecules into core-like particles and of VP2, VP3, VP5, and VP7 into virus-like particles (12, 13) provides a vehicle with which to investigate mutated VP7—particularly the function of the RGD motif in VP7. The report that VP7 in the virus is accessible to antibodies (10) suggests the presence of holes in the surface of the outer capsid. The structural data to date are consistent with RGD-integrin recognition being a common feature of an early stage of orbivirus infection, at least of insect cells, with different members of the genus presenting the recognition sequence in different structural contexts, perhaps modulating the integrin specificity. In the longer term, a study of core-like particles and virus-like particles with mutated VP7 may provide direct insight into the orbivirus host cell attachment and entry process.

ACKNOWLEDGMENTS

A.K.B. and P.G. contributed equally to this work.

We thank Yvonne Jones, Robert Esnouf, and Dave Stammers for help in data collection; N. Sakabe for making data collection at the Photon Factory possible; K. Harlos for in-house data collection support; and R. Bryan and R. Esnouf for computing facilities. We are grateful to S. Lee for help in the preparation of figures. We are grateful to R. Liddington for supplying the Mac-1 I domain coordinates.

A.K.B. and J.G. were supported by the BBSRC, and P.G. was supported by a grant from 'L'Association Française pour la Recherche Thérapeutique' between 1993 and 1994 and since then has been supported by the European Human Capital and Mobility Programme (ERBCHB1CT941689). The OCMS is supported by the BBSRC and MRC. This work is supported by BBSRC and NIH grants.

REFERENCES

1. **Acharya, R., E. Fry, D. Stuart, G. Fox, D. Rowlands, and F. Brown.** 1989. The three-dimensional structure of foot-and-mouth disease virus at 2.9 Å resolution. Nature (London) **337:**709–716.
1a. **Artymiuk, P.** Personal communication.
2. **Bairoch, A.** 1991. PROSITE: a dictionary of sites and patterns in protein. Nucleic Acids Res. **19:**2241–2245.
3. **Bairoch, A., and B. Boeckmann.** 1990. The SWISSPROT protein sequence bank. Nucleic Acids Res. **19:**2247–2248.

3a. **Basok, A. K., et al.** Unpublished results.
4. **Brünger, A. T., J. Kuriyan, and M. Karplus.** 1987. Crystallographic Rfactor refinement by molecular dynamic. Science **235:**23–28.
5. **Burroughs, J. N., R. S. O'Hara, C. J. Smale, C. Hamblin, A. Walton, R. Armstrong, and P. P. C. Mertens.** 1994. Purification and properties of virus particles, infectious subviral particles cores and VP7 crystals of African horsesickness virus serotype 9. J. Gen. Virol. **78:**1849–1857.
5a. **CCP4.** 1979. The SERC (UK) collaborative computing project no. 4, a suite of programs for protein crystallography. Daresbury Laboratory, Warrington, United Kingdom.
6. **Chotia, C., and A. M. Lesk.** 1986. The relation between the divergence of sequence and structure in proteins. EMBO J. **5:**823–826.
7. **Chuma, T., H. Le Blois, J. M. Sanchez Vizcaino, M. Diaz Laviada, and P. Roy.** 1992. Expression of the major core antigen VP7 of African horsesickness virus by a recombinant baculovirus and its use as a group-specific diagnostic reagent. J. Gen. Virol. **73:**925–931.
7a. **Collaborative Computational Project, Number 4.** 1994. The CCP4 suite: programs for protein crystallography. Acta Crystallogr. Sect. A **47:**110–119.
8. **Connolly, M. L.** 1983. Solvent-accessible surfaces of proteins and nucleic acids. Science **221:**709–713.
9. **Dyda, F., A. B. Hickman, T. M. Jenkins, A. Engelman, R. Craigie, and D. R. Davies.** 1994. Crystal structure of the catalytic domain of HIV-1 integrase: similarity to other polynucleotidyl transferases. Science **266:**1946.
10. **Eaton, B. T., A. R. Gould, A. D. Hyatt, B. E. H. Coupar, J. C. Martyn, and J. R. White.** 1991. A bluetongue serogroup-reactive epitope in the amino terminal half of the major protein VP7 is accessible on the surface of bluetongue virus particles. Virology **180:**687–696.
11. **Fox, G., N. R. Parry, P. V. Barnett, B. McGinn, D. J. Rowlands, and F. Brown.** 1989. The cell attachment site on foot-and-mouth disease virus includes the amino acid sequence RGD (arginine-glycine-aspartic acid). J. Gen. Virol. **70:**625–637.
12. **French, T. J., J. J. A. Marshall, and P. Roy.** 1990. Assembly of double-shelled, viruslike particles of bluetongue virus by the simultaneous expression of four structural proteins. J. Virol. **64:**5695–5700.
13. **French, T. J., and P. Roy.** 1990. Synthesis of bluetongue virus (BTV) corelike particles by a recombinant baculovirus expressing the two major structural core proteins of BTV. J. Virol. **64:**1530–1536.
14. **Grimes, J.** 1995. Structural studies on bluetongue virus. Ph.D. thesis. Oxford University.
15. **Grimes, J., A. K. Basak, P. Roy, and D. Stuart.** 1995. The crystal structure of bluetongue virus VP7. Nature (London) **373:**167–170.
15a. **Grimes, J., and D. Stuart.** Unpublished program.
16. **Howell, P. G.** 1962. The isolation and identification of further antigenic types of African horsesickness virus. Onderstepoort. J. Vet. Res. **29:**139–149.
17. **Hutchinson, E. G., and J. M. Thornton.** 1990. HERA—a program to draw schematic diagrams of protein secondary structures. Proteins Struct. Funct. Genet. **8:**203–212.
18. **Iwata, H., T. Chuma, and P. Roy.** 1992. Characterization of genes encoding two of the major capsid proteins of epizootic haemorrhagic disease virus indicates a close genetic relationship to bluetongue virus. J. Gen. Virol. **73:**915–925.
19. **Jancarik, J., and S. H. Kim.** 1991. Sparse matrix sampling: a screening method for crystallization of proteins. J. Appl. Crystallogr. **24:**409–411.
20. **Jones, E. Y., K. Harlos, M. J. Bottomley, R. C. Robinson, P. C. Driscoll, R. M. Edwards, J. M. Clements, T. J. Dudgeon, and D. I. Stuart.** 1995. Crystal structure of an integrin-binding fragment of vascular cell adhesion molecule-1 at 1.8 Å resolution. Nature (London) **373:**539–544.
21. **Jones, E. Y., and D. I. Stuart.** 1991. Locating heavy atom sites by automatic Patterson search—GROPAT, p. 39–47. *In* W. Wolf, P. R. Evans, and A. G. W. Leslie (ed.), Isomorphous replacement and anomalous scattering. Science and Engineering Research Council, Warrington, United Kingdom.
22. **Kabsch, W.** 1988. Automatic indexing of rotation diffraction patterns. J. Appl. Crystallogr. **21:**67–71.
23. **Kabsch, W.** 1988. Evaluation of single crystal X-ray diffraction data from a position sensitive detector. J. Appl. Crystallogr. **21:**916–924.
24. **Kabsch, W., and C. Sander.** 1983. Dictionary of protein secondary structure: pattern recognition of hydrogen-bonded and geometrical features. Biopolymers **22:**2577–2637.
25. **Kleywegt, G., and T. A. Jones.** 1994. Detection, delineation, measurement and display of cavities in macromolecular structures. Acta Crystallogr. Sect. D **50:**178–185.
26. **Kraulis, P. J.** 1991. MOLSCRIPT: a program to produce both detailed and schematic plots of protein structure. J. Appl. Crystallogr. **24:**946–950.
27. **Kyte, J., and R. Doolittle.** 1982. A simple method for displaying the hydropathic character of a protein. J. Mol. Biol. **157:**105–132.
28. **Laviada, M. D., P. Roy, and J. M. Sanchez-Vizcaino.** 1992. Adaptation and evaluation of an indirect ELISA and immunoblotting test for African horsesickness antibody detection, p. 646–650. *In* T. E. Walton and B. I. Osburn (ed.), Bluetongue African horsesickness and related orbiviruses. CRC Press, Boca Raton, Fla.
29. **Le Blois, H., and P. Roy.** 1993. A single point mutation in the VP7 major core protein of bluetongue virus prevents the formation of core-like particles. J. Virol. **67:**353–359.
30. **Lee, J., P. Rieu, M. A. Arnaout, and R. Liddington.** 1995. Crystal structure of the A domain from the a subunit of integrin CR3 (CD11b/CD18). Cell **80:**631–638.
31. **Leslie, A. G. W.** 1987. Profile fitting, p. 39–50. *In* J. H. Helliwell, P. A. Machin, and M. Z. Papiz (ed.), Computational aspect of protein crystal data analysis. SERC, Daresbury Laboratory, Warrington, United Kingdom.
32. **Logan, D., R. Abu-Ghazaleh, W. Blakemore, S. Curry, T. Jackson, A. King, S. Lea, R. Lewis, J. Newman, N. Parry, D. Rowlands, D. Stuart, and E. Fry.** 1993. Structure of a major immunogenic site on foot-and-mouth disease virus. Nature (London) **362:**566–568.
33. **Lubroth, J.** 1988. African horsesickness and the epizootic in Spain 1987. Equine Pract. **10:**26–33.
34. **Luzatti, V.** 1952. Traitement statistique des erreurs dans la détermination des structures cristallines. Acta Crystallogr. **5:**802–810.
35. **Mason, P. W., E. Rieder, and B. Baxt.** 1994. RGD sequence of foot-and-mouth disease virus is essential for infecting cells via the natural receptor but can be bypassed by an antibody-dependent enhancement pathway. Proc. Natl. Acad. Sci. USA **91:**1932–1936.
36. **Matthews, B. W.** 1985. Determination of protein molecular weight, hydration, and packing from crystal density. Methods Enzymol. **114:**176–187.
37. **McIntosh, B. M.** 1958. Immunological types of horsesickness virus and their significance in immunization. Onderstepoort J. Vet. Res. **27:**465–538.
38. **McPherson, A. J.** 1982. Preparation and analysis of protein crystals, p. 82–160. John Wiley and Sons, New York.
39. **Mellor, P.** 1993. African horsesickness transmission and epidemiology. Vet. Res. **24:**199–212.
40. **Merrit, E. A., and M. E. P. Murphy.** 1994. Raster3D version 2.0. A program for photo-realistic molecular graphics. Acta Crystallogr. Sect. D **50:**869–873.
40a. **Mertens, P. P. C.** Personal communication.
41. **Mertens, P. P. C., J. N. Burroughs, H. Fu, M. P. Wellby, D. M. Jennings, R. S. O'Hara, A. Walton, and P. S. Mellor.** Enhanced infectivity of modified bluetongue virus particles for Culicoides vectors and to infect cell lines. Virology, in press.
42. **Murphy, F. A., E. C. Borden, R. E. Shope, and A. Harrison.** 1971. Physicochemical and morphological relationships of some arthropod-borne viruses to bluetongue virus—a new taxonomic group. Electron microscopic studies. J. Gen. Virol. **13:**273–288.
43. **Navaza, J.** 1992. AMoRe: a new package for molecular replacement, p. 87–90. *In* E. J. Dodson, S. Gover, and W. Wolf (ed.), Molecular replacement. SERC, Daresbury Laboratory, Warrington, United Kingdom.
44. **Otwinowski, Z.** 1991. Maximum likelihood refinement of heavy atom parameters, p. 80–85. *In* W. Wolf, P. R. Evans, and A. G. W. Leslie (ed.), Isomorphous replacement and anomalous scattering. SERC, Daresbury Laboratory, Warrington, United Kingdom.
45. **Otwinowski, Z.** 1993. Oscillation data reduction program, p. 56–62. *In* L. Sawyer, N. Isaac, and S. Bailey (ed.), Data collection and processing. SERC, Daresbury Laboratory, Warrington, United Kingdom.
46. **Pierschbacher, M. D., and E. Ruoslahti.** 1984. Cell attachment activity of fibronectin can be duplicated by small synthetic fragments of the molecule. Nature (London) **309:**30–33.
47. **Prasad, B. V. V., S. Yamaguchi, and P. Roy.** 1992. Three-dimensional structure of single-shelled bluetongue virus. J. Virol. **66:**2135–2142.
48. **Robinson, I. K., and S. C. Harrison.** 1982. Structure of the expanded state of tomato bushy stunt virus. Nature (London) **297:**563–568.
49. **Rossmann, M. G., et al.** 1985. Structure of a human common cold virus and functional relationship to other picornaviruses. Nature (London) **317:**145–153.
50. **Roussel, A., and C. Cambillau.** 1989. TURBO-FRODO, p. 77–78. *In* Silicon Graphics (ed.), Silicon graphics geometry partner directory. Silicon Graphics, Mountain View, Calif.
51. **Roy, P.** 1992. Bluetongue virus proteins. J. Gen. Virol. **73:**3051–3064.
52. **Roy, P.** Orbiviruses and their replication. *In* B. N. Fields (ed.), Virology, in press. Raven Press, New York.
53. **Roy, P., T. Hirasawa, M. Fernandez, V. M. Blinov, and J. M. Sanchez-Vixcaino Rodrique.** 1991. The complete sequence of the group-specific antigen, VP7, of African horsesickness disease virus serotype 4 reveals a close relationship to bluetongue virus. J. Gen. Virol. **72:**1237–1241.
54. **Roy, P., J. J. Marshall, and T. J. French.** 1990. Structure of the bluetongue virus genome and its encoded proteins. Curr. Top. Microbiol. Immunol. **162:**43–87.
55. **Ruoslahti, E.** 1988. Fibronectin and its receptors. Annu. Rev. Biochem. **57:**375–413.
56. **Sakabe, N.** 1991. X-ray diffraction data collection system for modern protein crystallography with a Weissenberg camera and an imaging plate using synchrotron radiation. Nucl. Instr. Methods Phys. Res. **303:**448–463.
57. **Stuart, D. I., and E. Y. Jones.** 1993. Weissenberg data collection for macromolecular crystallography. Curr. Opin. Struct. Biol. **3:**737–740.
58. **Zlotnick, A., V. S. Reddy, R. Dasgupta, A. Schneemann, W. J. Ray, Jr., R. R. Rueckert, and J. E. Johnson.** 1994. Capsid assembly in a family of animal viruses primes an autoproteolytic maturation that depends on a single aspartic acid residue. J. Biol. Chem. **269:**13680–13684.

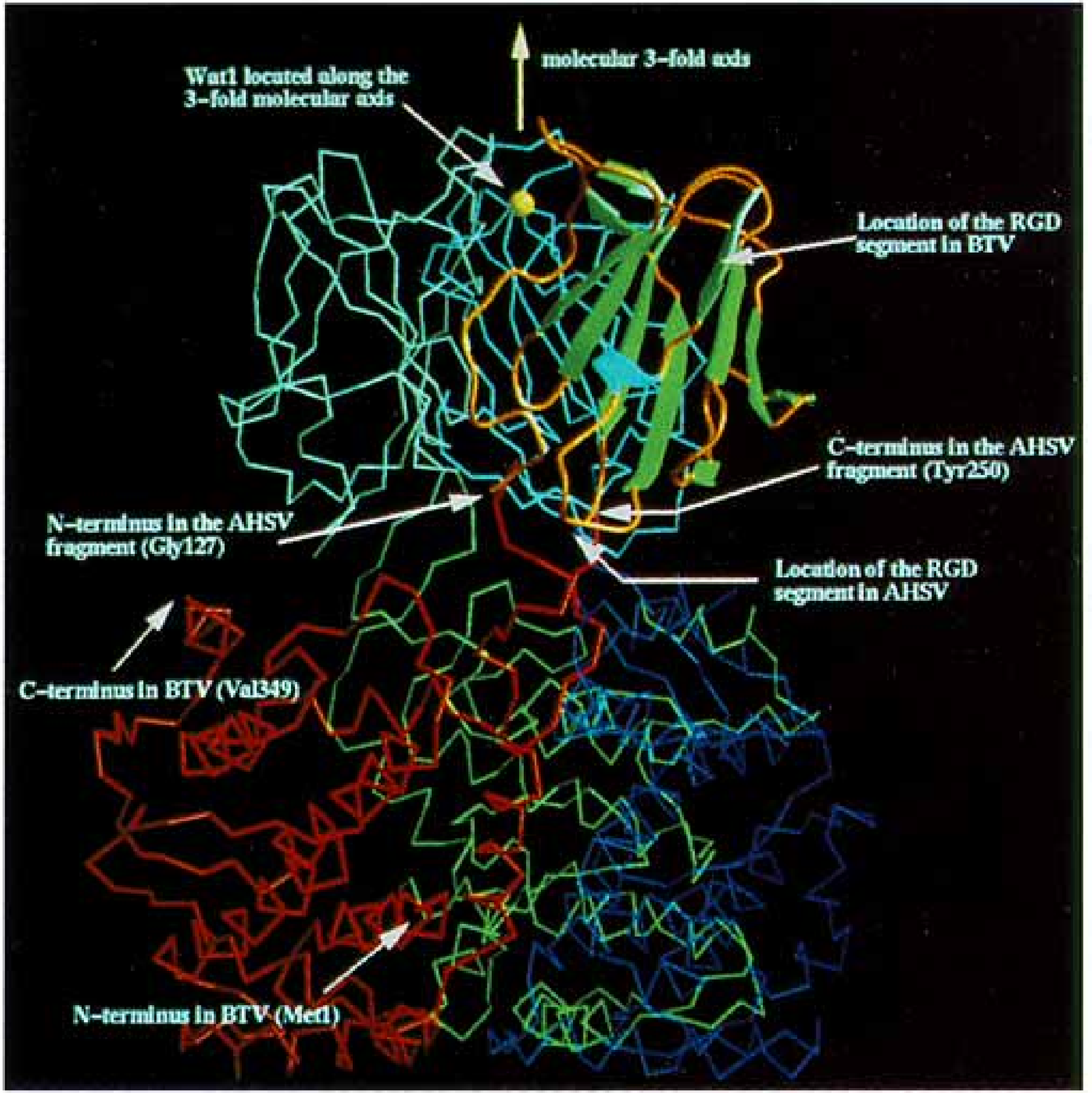
molecular 3-fold axis
Wat1 located along the 3-fold molecular axis
Location of the RGD segment in BTV
C-terminus in the AHSV fragment (Tyr250)
N-terminus in the AHSV fragment (Gly127)
Location of the RGD segment in AHSV
C-terminus in BTV (Val349)
N-terminus in BTV (Met1)

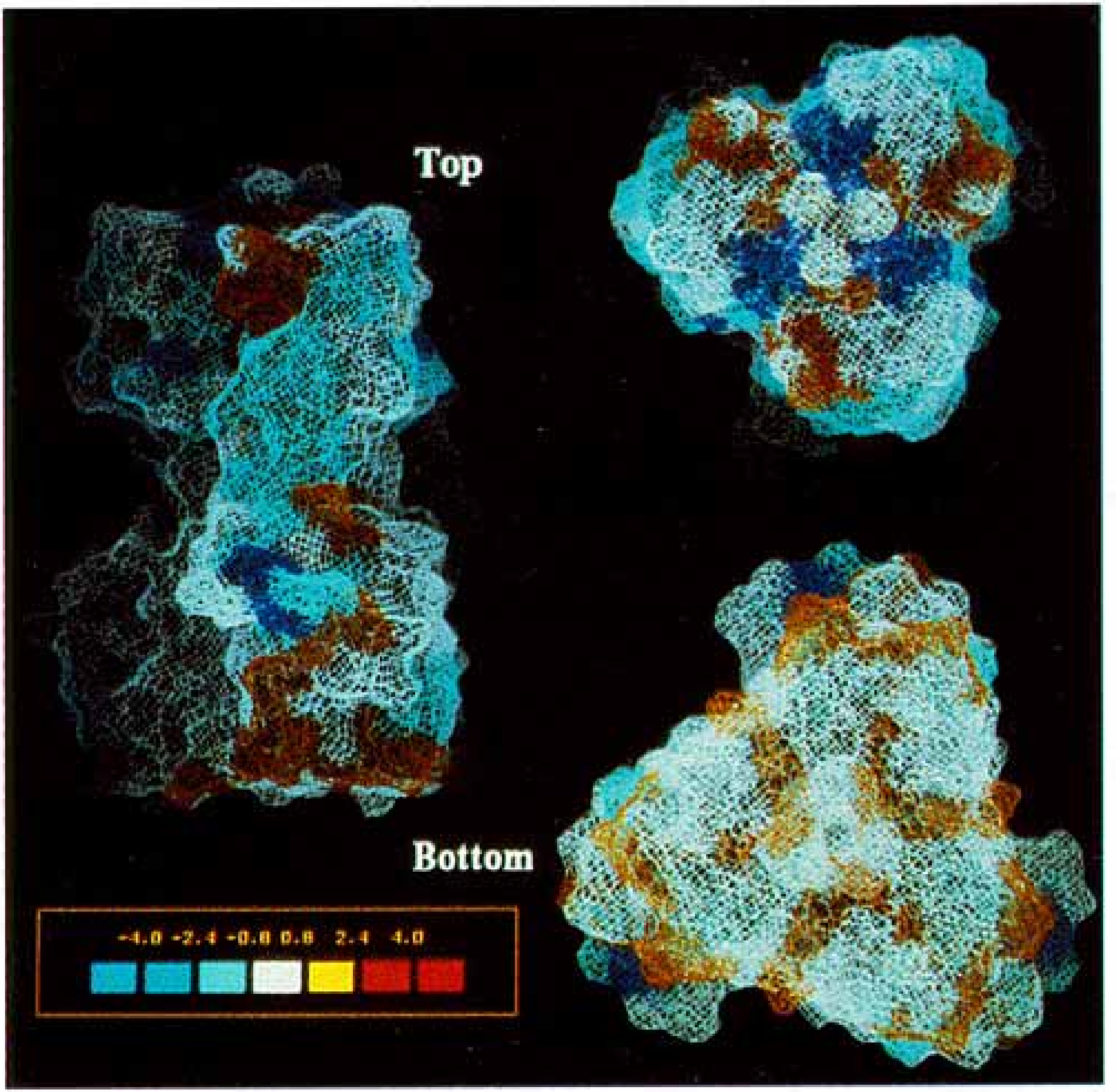
Top
Bottom
-4.0 -2.4 -0.8 0.8 2.4 4.0

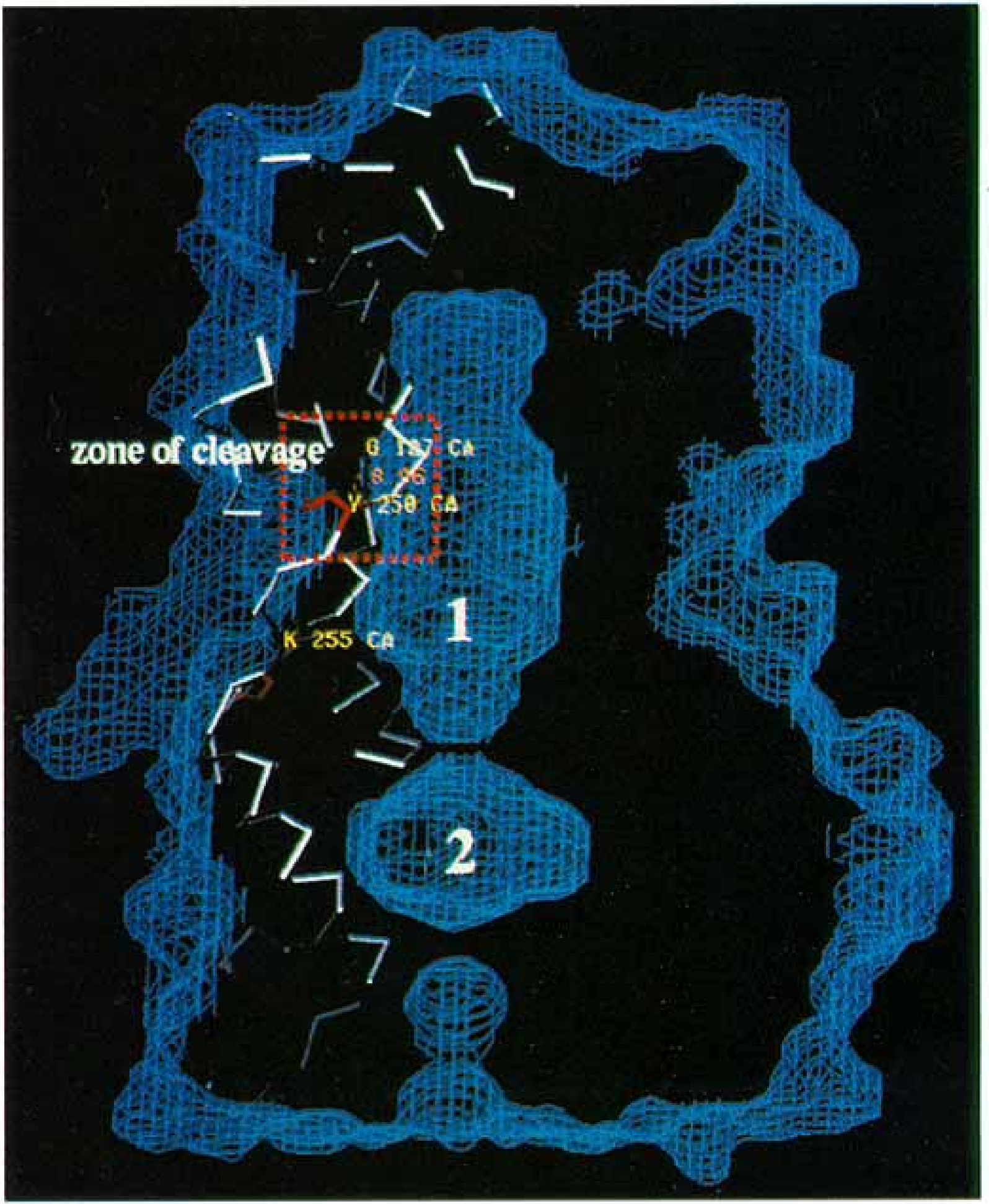
zone of cleavage
G 197 CA
R 96
Y 250 CA
K 255 CA
1
2